Down-regulation of the Androgen Receptor by G-quadruplex Ligands Sensitizes Castration-resistant Prostate Cancer Cells to Enzalutamide

Martina Tassinari,[§,‡] Graziella Cimino-Reale,[†,‡] Matteo Nadai,[§] Filippo Doria,[#] Elena Butovskaya,[§] Marta Recagni,[†] Mauro Freccero,[#] Nadia Zaffaroni,[†] Sara N. Richter,[§,] Marco Folini[†,*]*

[§]Department of Molecular Medicine, University of Padua, via A. Gabelli 63, 35121 Padua, Italy.

[†]Department of Applied Research and Technological Development, Fondazione IRCCS Istituto Nazionale dei Tumori di Milano, Via G.A. Amadeo 42, 20133 Milan, Italy.

[#]Department of Chemistry, University of Pavia, v. le Taramelli 10, 27100, Pavia, Italy.

KEYWORDS. Androgen receptor; Castration resistant prostate cancer; Enzalutamide; G-quadruplex; Naphthalene diimide; Promoter.

ABSTRACT. Stabilization of the G-quadruplexes (G4s) within the androgen receptor (AR) gene promoter to block transcription may represent an innovative approach to interfere with aberrant AR signaling in castration resistant prostate cancer (CRPC). A library of differently functionalized naphthalene diimides (NDIs) was screened for their ability to stabilize AR G4s: the core-extended

NDI (**7**) stood out as the most promising ligand. AR-positive cells were remarkably sensitive to **7** in comparison to AR-negative CRCP or normal prostate epithelial cells; **7** induced remarkable impairment of AR mRNA and protein amounts and significant perturbations in the expression levels of KLK3 and of genes involved in the activation of AR program via feedback mechanisms. Moreover, **7** synergistically interacted with Enzalutamide, an inhibitor of AR signaling used in second-line therapies. Overall, our data show that stabilization of AR G4s may represent an alternative treatment options for CRPC and other malignancies relying on aberrant androgen signaling.

INTRODUCTION. Prostate cancer (PCa) is one of the most commonly diagnosed cancers among men in Western countries and the second leading cause of cancer-related death.[1] Despite local treatments (i.e., radical prostatectomy, external radiotherapy and brachytherapy) are successful for disease eradication, approximately 20-35% of patients with localized/locally-advanced PCa experience disease relapse (i.e., biochemical failure) with or without evidence of metastases.[2,3]

The androgen deprivation therapy (ADT), which is based on surgical or chemical castration,[2] has been established as the standard of care systemic therapy for patients with recurrent, progressive or metastatic androgen-sensitive disease after local treatment.[4] However, though ADT provides good disease control, castration-resistant prostate cancer (CRPC) nearly invariably develops, eventually leading to the lethal form of the disease referred to as metastatic castration resistant PCa (mCRPC).[3] Although curative treatments for mCRPC are not available yet, different therapeutic options have been established for CRPC patients, such as taxane-based (docetaxel, cabazitaxel) chemotherapy, immunotherapy (sipuleucel-T) and bone-targeting radiotherapy (radium-223).[5] Moreover, it is indisputable today that CRPC is not an androgen-

independent/hormone-refractory disease state,[1,2] as it continues to be dependent on androgen receptor (AR) signaling via multiple mechanisms.[1,2] This evidence has provided the rationale for the implementation of second-generation agents for ADT-based interventions, among which Enzalutamide (an AR receptor inhibitor) and Abiraterone acetate (an inhibitor of androgen biogenesis) have been approved for the treatment of mCRPC.[1,2] However, resistance mechanisms relying on the maintenance of the AR signaling, which include AR gene amplification, point mutations, expression of constitutively active AR splice variants and altered intratumoral androgen synthesis,[1,2] have been documented also for these second-generation therapeutic agents.[1]

As a consequence, improving our understanding of the biological bases of the castration resistant phenotype and the development of novel therapeutic interventions to counteract AR resistance are main issues that urgently warrant to be addressed. In this context, it has been proposed that the interference with AR gene transcription would represent a suitable approach to overcome the resistance mechanisms based on aberrant AR signaling.[6]

G-quadruplexes (G4s) are non-canonical nucleic acids secondary structures that may form in single-stranded G-rich sequences under physiological conditions.[7] The quadruplex basic structure is the G-quartet and consists of four guanines held together via Hoogsteen-type hydrogen bonds base-pairing. Two or more quartets stack on top of each other to form the G4. The presence of K^+ cations specifically supports G4 formation and stability. G4s are highly polymorphic, in terms of strand stoichiometry (forming both inter- and intramolecular structures), strand orientation/topology and loop sequence, length and position.[8] G4s have been shown in humans and other eukaryotes,[9,10] in prokaryotes[11–16] and in viruses.[17–19] From a functional point of view, G4s in eukaryotes have been reported to be involved in key regulatory and pathological roles, including transcriptional modulation of gene promoters and enhancers, telomere extension and

maintenance, translation, chromatin epigenetic regulation, DNA recombination.[18,20–24] *In vivo* formation of G4s has been consolidated by the development of G4 specific antibodies[25,26] and the discovery of cellular proteins that specifically process G4s.[27–29]

In this context, a G4 forming sequence (Figure 1A) has been identified and characterized within the AR gene promoter,[6] thus suggesting that binding and stabilization of such G4 structure by specific ligands may represent an alternative approach to available therapeutic options for interfering with aberrant androgen signaling in CRPC.[6,30]

G4 binders and stabilizers are often characterized by aromatic cores with protonable side chains, and include acridines,[31,32] porphyrins,[31] fluoroquinolones,[33] anthraquinones, phenanthrolines, quinacridines, carbazoles, bis-indole carboxamides, triazoles, benzimidazoles,[34] pyridostatin,[35] naphthalene diimides (NDIs)[36–42] and natural compound derivatives, such as berberines,[43] telomestatin[44] and quindolines.[45] Among them, NDIs form an entire library of G4 ligands due to flexible synthetic protocols, which allow the introduction of four different side chains on the NDI core. Such a structural diversification can be exploited for a chemical conjugation strategy, which is useful to implement binding affinity, solubility, and cellular uptake. Moreover, the extension of the NDI core offers an opportunity to enhance both G4 binding potency and selectivity. In fact, core-extended NDIs (c-exNDIs) are potent G4 binders displaying anti-HIV-1 activity due to their ability to bind viral G4s with high affinity.[41]

In the present investigation, we have explored the possibility to block AR transcription by stabilizing the G4s within the AR promoter. We preliminarily screened a small library of functionalized NDI derivatives as AR-G4 ligands by Fluorescence Resonance Energy Transfer (FRET). The binding of the most promising ligand was further investigated through biochemical and biophysical assays. Moreover, the NDI derivative caused a remarkable decrease in the

expression level of both AR mRNA and protein amounts in CRPC cells, and modulated the expression of genes reported to be regulated by AR and involved in key biological processes. Overall, our data provided the rationale for the future development of alternative treatment for CRPC, based on G4 recognition and stabilization.

RESULTS.

Chemistry. We have selected four different types of NDI derivatives from our in-house library: a) four di- and tricationic substituted NDIs (**1-3** and **5**), b) a monocationic tetra-substituted NDI (**4**), c) two core extended NDIs (**6**,**7**) and d) two novel polycationic NDI-dyads (**8**,**9**). The aim was to evaluate the effects of the extension of the aromatic core, oxidation state and the presence of dimeric binding units on G4 binding and toxicity, keeping similar side-chain length and the identical solubilizing terminal moiety ($NHMe_2^+$). NDIs **1-7** have been previously synthesized and characterized.[38,39,41,46–49] NDI-dyads **8** and **9** are novel ligands and they have been prepared according to the synthetic protocol outlined in Scheme 1. In detail, we used the same synthetic protocol for both NDIs **11** and **12**, using 1,4-diaminobutane and 1,7-diaminoheptane, respectively, as amines for the nucleophilic aromatic substitution. The latter step was optimized in order to achieve the dehalogenated ligands in a one-pot synthesis, yielding both **8** and **9** as major products.

Screening of G4-binding NDIs by FRET melting assay and SPR analysis. We evaluated NDIs **1-9** (Figure 1B) for their ability to bind the G4s forming in the minimal promoter sequence of AR.[6] Considering that multiple G4s may form in this region (Figure 1A), the least polymorphic G4 (i.e. AR3)[6] and the full-length G4 forming sequence (i.e. AR1) were used in FRET melting assay, which allows assessing G4 stabilization upon compounds binding. The fluorophore end-labeled AR3 sequence displayed a melting temperature $T_{1/2}$ of 54.5 ± 0.4 °C in the absence of any

NDIs, while labeled AR1 showed a $T_{1/2}$ of 69.9 ± 0.1 °C. In the presence of c-exNDI **7** (Figure 1B), $T_{1/2}$ increased by 31.0 ± 0.9 °C and 20.5 ± 0.7 °C, respectively (Figure S1A and C, Table 1), making c-exNDI **7** the best AR G4 stabilizing compound. The NDI-dyads (**8**, **9**; Figure 1B) displayed also very good stabilization properties (AR3 $\Delta T_{1/2}$ 17.0-19.7 °C, AR1 $\Delta T_{1/2}$ 8.3-11.3 °C, Figure S1A and C, Table 1), while tri-substituted NDIs, (**1**-**3** and **5**; Figure 1B) presenting side chains with terminal NMe_2 moieties, were less effective stabilizers (AR3 $\Delta T_{1/2}$ 9.0-13.0 °C, AR1 $\Delta T_{1/2}$ 4.5-11.0 °C, Figure S1A and C, Table 1). The c-exNDI derivative (**6**; Figure 1B) lacking the fourth condensed benzene ring showed even lower stabilization (AR3 $\Delta T_{1/2}$ 6.0 ± 0.8 °C, AR1 $\Delta T_{1/2}$ 3.6 ± 0.3 °C, Figure S1A and C, Table 1), whereas the tetra-substituted NDI (**4**; Figure 1B) was unable to stabilize AR G4s (Figure S1A and C, Table 1), likely due to lack of planar geometry.[48] To check NDI selectivity for G4 *vs.* duplex, FRET analysis was also performed on dsDNA (Figure S1E, Table 1). All NDI derivatives, with except to 1, were basically devoid of stabilizing effect on dsDNA. For compound **7**, ΔT_m were also calculated as the minimum of the first derivative curve, and results were in line with $\Delta T_{1/2}$..

Surface plasmon resonance (SPR) analysis was next used to measure the compounds' binding affinity to the AR1 sequence. Data were fitted using the Affinity – Steady State model and are reported in Table 2. Compound **7** was confirmed to be the best binder among the series, with a K_D for AR1 G4 of 17.9 ± 2.0 nM, while a single stranded DNA made of a scrambled sequence of the same length of AR1 in which five guanines were mutated to thymines (Table S1) was bound less efficiently (K_D 195.7 ± 18.0 nM, Figure 2).

Assessment of the biological activity of NDIs in CRPC cells. The biological activity of NDI derivatives was preliminarily evaluated on a panel of CRPC cells, which included the 22Rv1 cell

line, derived from a primary PCa that was xenografted and serially propagated in mice after castration-induced regression and relapse of the parental, androgen-dependent CWR22 xenograft,[50,51] as well as DU145 and PC-3 cell lines derived from a PCa brain and bone metastasis, respectively.[50,51] Of note, though the three cell lines show a castration-resistant phenotype,[1] 22Rv1 cells retain AR transcription and are characterized by the H875Y point mutation within the ligand-binding domain of the full length AR (AR-FL, Table 3), as well as by the expression of at least two AR variants (AR-Vs, Table 3), one that originates by the duplication of exon 3 and the other that is a C-terminally truncated, constitutively active form of the receptor.[50,51] Conversely, DU145 and PC-3 cells are characterized by loss of AR expression (Table 3).[1,51] In addition, the hormone naïve LNCaP cell line, bearing the T877A point mutation in the AR gene[51] and the non-tumorigenic, SV40-immortalised AR-negative normal adult prostatic epithelial PNT1A cells[52,53] were also included (Table 3).

Exposure of cells to increasing concentrations (0.0001-10 μM) of tested compounds resulted in a cytotoxic effect, with IC_{50} values (i.e., concentration of ligand leading to 50% inhibition of cell viability calculated from the dose-response curves) ranging from micromolar to nanomolar range (Table 3). In particular, amongst the tested derivatives, **2** and **7** exerted a marked cytotoxic activity across the tested cell lines compared to the other compounds belonging to the series (Table 3). However, **7** resulted to be more active than compound **2** (Figure S2A), which was previously characterized as a good telomeric and promoter G4 binder in several cancer cell models[47,48]. In fact, despite both compounds had a similar cytotoxic effect on PNT1A normal prostate epithelial cells (Table 3 and Figure S2A), the ratio between the IC_{50s} revealed a 4-10-fold higher activity of **7** with respect to **2** in PCa cells, hence defining a good therapeutic window. Moreover, compound **7** exerted a remarkable cytotoxic activity in 22Rv1 cells (Table 3) that are castration resistant as a

consequence of the persistent activation of the AR signaling due to the expression of constitutively active variants of AR[50,51]. Of note, such a superior cytotoxic effect of **7** was not ascribable to differences in cellular uptake among normal or PCa cells, as evidenced by the assessment of drug internalization using fluorescence microscopy (Figure S2B). In addition, the exposure of 22Rv1 cells to compound **7** resulted in a marked reduction of AR-FL and AR-Vs protein amounts with respect to cells exposed to an equitoxic amount of compound **2** (Figure S2C).

Derivative 7 inhibits AR gene transcription and efficiently binds and stabilizes AR G4. The superior activity of **7** observed in the AR-positive CRPC cells, both in terms of inhibition of cell viability and impairment of AR protein amounts, prompted us to investigate the impact of **7** on AR expression at transcriptional and translational level. Specifically, real-time RT-PCR assessment of AR transcript revealed that, despite time-dependent fluctuations in the basal expression of AR mRNA were appreciable in cells treated with compound **4** (IC_{50}), which is devoid of AR G4 stabilization abilities (Table 1) and was the least active compound across the tested cell lines (Table 3 and Figure S2A), a significant reduction of AR mRNA was observed over time in 22Rv1 cells (Figure 3A) exposed to an equitoxic amount of **7** (IC_{50}). Such an effect was paralleled by a remarkable down-regulation of the mRNA of *KLK3* (Figure 3A), a chief AR-regulated gene encoding for the prostate specific antigen (PSA). Similar results were obtained in the hormone naïve, AR-positive LNCaP cell line, though **7**-mediated decrease in AR and KLK3 mRNA levels was transient, with a major inhibitory effect on the transcription of both genes at 48 h and a partial recovery of the mRNA expression levels 24 h later (Figure 3A).

Furthermore, compared to untreated or **4**-treated 22Rv1 cells, **7**-mediated inhibition of AR gene transcription was accompanied by a marked reduction over time of both AR-FL and AR-Vs protein

amounts (Figure 3B, C). Similarly, a significant decrease in AR-FL protein abundance, which was paralleled by a marked reduction in PSA levels, was observed in **7**- compared to **4**-treated or untreated LNCaP cells (Figure 3B, C). According to literature data[51], no PSA protein was readily detectable in 22Rv1 cells (Figure 3B, C).

Based on these findings, the binding properties of **7** to AR G4s were further investigated. The ability of **7** to highly stabilize AR G4s was confirmed by circular dichroism (CD). The unlabeled AR3 sequence had a T_m of 78.8 ± 1.7 °C. The discrepancy with the end-labelled AR3 sequence measured by FRET is likely due to the presence of the fluorophores at the 5'- and 3'-end of the sequence that destabilize G4 folding.[54] Compound **7** greatly stabilized AR3 G4 to T_m > 90 °C (Figure 4). A similar stabilizing activity (T_m > 90 °C) was obtained with AR1, which had T_m of 74.9 ± 0.3 °C when not bound to the compound (Figure 4). CD thermal unfolding analysis was also performed on the control ssDNA (Table S1) made of a scrambled sequence of the same length of AR1 in which five guanines were mutated to thymines. Because the original AR1 sequence is so rich in Gs, this oligonucleotide retained the ability to fold into G4, whereas to a lesser extent, as shown by the less straightforward G4 signature in the CD spectrum (Figure S3). In addition, a double stranded DNA (dsDNA, Table S1), obtained by annealing equimolar amounts of ssDNA and its complementary sequence (ssDNA compl, Table S1), was used as control. Upon addition of **7**, a minor stabilization of ssDNA and dsDNA was detected: ΔT_m were 4.7 ± 1.5 °C and 2.7 ± 0.1 °C, respectively. Interestingly, no conformational changes were observed on both control oligonucleotides. The observed stabilization is likely due to the electrostatic interactions of **7**, which is positively charged, with the negatively charged DNA counterpart; however, the fact that no conformational changes were observed, indicates no specific sites of interaction of **7** to the ssDNA and dsDNA.

To check if NDI **7** was able to inhibit polymerase progression at the G4 site, an extended AR1 sequence was used and the *Taq* polymerase stop assay was performed. In the absence of the compound and in the presence of 10 mM K^+, two weak pausing sites were visible. These corresponded to G-tracts IV and V (lane 2, Figure 5A), indicating that K^+ stimulates G4 folding in the extended AR1 template. Upon addition of increasing concentrations of **7**, the two stop sites augmented in intensity, while the full-length amplification product steadily decreased (lanes 3-5, Figure 5A and B). In contrast, **7** had no effect on the control ssDNA template (Table S1) thus indicating that the observed polymerase inhibition was G4-dependent (lanes 8-10, Figure 5A).

The exposure of AR-positive CRPC cells to 7 result in perturbations of gene expression and in a synergistic pharmacological interaction with Enzalutamide.

The analysis of the expression levels of 92 genes commonly associated with the molecular mechanisms of cancer development and progression revealed that 16, 18 and 12 genes were significantly ($P < 0.05$) modulated (cut-off: fold-change $\geq |1.5|$) in 22Rv1, PC-3 and DU145 cells, respectively, upon a 48-h exposure to **7** (IC_{50}) with respect to untreated cells (Figure 6A and Table S2). Among these differently expressed genes only 2 (*ITGB3*, *MAX*) and 1 (*WNT1*) genes were down- and up-modulated, respectively, in all three cell lines (Figure 6A and Table S2). Strikingly, among differently expressed genes in NDI-treated *vs.* untreated 22Rv1 cells ($P < 0.05$; cut-off: fold-change $\geq |1.5|$) showing a trend towards an opposite modulation in AR-negative (PC-3 and DU145) cells (Table S2), we found a significant modulation of genes known for being regulated by the AR[55,56] or that are involved in the activation of AR program via feedback mechanisms[57]. These included factors belonging to the PI3K/AKT/mTOR pathway (i.e., *AKT1* and *PTEN*) and the *ERBB2/HER2/Neu* tyrosin kinase receptor (Figure 6A). Moreover, a remarkable down-

modulation of genes involved in the G1/S-phase transition during the cell cycle progression (i.e., *CCND1*, *CCNE1*) was observed along with a transcription program in favor of apoptosis induction, as suggested by the up-modulation of the pro-apoptotic *BAX* gene and the down-modulation of the anti-apoptotic *BCL-2* gene (Figure 6A and Table S2). Conversely, no major differences in the expression levels of *MYC* (a well renowned and validated G4-regulated gene)[58] and *JUN*, both of which acting as upstream regulators of AR transcription[6], were found in 22Rv1 compared to PC-3 and DU145 cells upon exposure to **7** (Table S2). Furthermore, in keeping with the evidence that telomerase - the enzyme responsible for the attainment of cancer cell immortality - is positively regulated by AR[59], we found that NDI-treated 22Rv1 cells were also characterized by a significant inhibition of telomerase activity (Figure 6B).

To explore the possibility that **7** may interact with drugs clinically relevant for CRPC, 22Rv1 and PC-3 cells were exposed to the compound in combination with Enzalutamide (MDV3100), an inhibitor of AR signaling used in second-line ADT for mCRPC.[1,2] A marked synergistic interaction was observed in 22Rv1 cells treated with Enzalutamide in combination with compound **7**, as suggested by the shift of the dose-response curve compared to single agent treatments (Figure 6C) and by a combination index (CI, calculated according to Chou & Talaly's method at a dose effecting (ED) 50% and 75% of cell viability) < 1 at both ED_{50} (0.29 ± 0.02) and ED_{75} (0.37 ± 0.03). Moreover, CI-Fa plot clearly shows that the CI was always <0.5 at all tested concentrations (Figure 6D), thus indicating a strong synergistic interaction between the two agents. Of note, **7**-treated 22RV1 cells were characterized by a marked reduction in the basal and phosphorylated levels of AKT1 as well as of Cyclin D1 protein amounts (Figure 6E), which are determinants for the activation of AR program via a feedback mechanism[57,60] and for the resistance of PCa cells to Enzalutamide,[61] respectively. Conversely, PC-3 cells were not sensitized to Enzalutamide in the

presence of **7** as evidenced by the dose-response curves (Figure 6D) and by the CI-Fa plot, which indicated a remarkable trend toward an antagonistic interaction, with CI values > 1 already at an Fa < 0.5 (Figure 6E) and at both ED_{50} (2.18 ± 0.24) and ED_{75} (21.1 ± 4.1).

DISCUSSION AND CONCLUSION. The interference with AR signaling by means of ADT has represented the first-line treatment for locally advanced or metastatic PCa.[62] However, though initially effective, ADT does not represent a curative approach as the vast majority of PCa patients on ADT undergo disease relapse followed by progression to a castration-resistant disease.[63] Accumulating evidence has indicated that, in spite of castration levels of androgens upon ADT, the AR signaling remains active and plays a critical role in CRPC.[64] The contribution of AR to the development of CRPC was underscored by the pioneer observation that *AR* gene amplification occurred in nearly one third of mCRPC patients but not in matched tumor specimens obtained prior ADT.[65] Whole genome analyses have recently confirmed this observation thus contributing to reinforce the central role of AR signaling pathway in the progression of PCa.[64,66]

Mechanisms that may contribute to the reactivation of AR signaling in CRPC include AR gene amplification, gain-of-function mutations, expression of constitutively active splicing variants, intratumoral androgen synthesis as well as changes in AR post-translational modifications and the presence of altered levels of cofactors that interact with and modulate the activity of AR and of its downstream targets.[64] Overall, these findings indicate that AR still represents a viable target in CRPC patients.

Given that AR-Vs plays a pivotal role in sustaining the castration resistant phenotype[63] and that no significant somatic mutations within the promoter of AR gene have been reported thus far,[6] the possibility to interfere with AR gene transcription appears an intriguing approach for the

development of novel therapeutic strategies to circumvent the documented, AR signaling-dependent mechanisms of resistance to castration in CRPC.

In the present study we pursued an approach to interfere with AR expression in experimental models of CRPC based on the rationale that a G4 forming sequence has been characterized in the AR promoter, which can be targeted by specific ligands, with consequent downregulation of transcription.[6]

In order to identify molecules that bind and stabilize the AR G4s, a FRET melting screen on a NDI-based small library was performed on the least polymorphic AR G4, i.e. AR3, and on the full length-sequence, i.e. AR1, and SPR analysis was employed to calculate K_D values. In particular, the monocationic tetra-substituted NDI, **4**, was unable to stabilize both AR G4s, because of lack of planar geometry. Di- and tricationic substituted NDIs, **1**-**3** and **5**, were mild stabilizer, while polycationic NDI-dyads , **8** and **9**, displayed very good binding properties. The most promising derivate was compound **7**, which highly increased the stability of both AR1 and AR3 oligonucleotides, as assessed by FRET analysis. In addition, SPR data indicated high binding affinity of **7** to AR1 G4 (K_D value in the low nanomolar range). This is consistent with the fact that **7** is a c-exNDI, characterized by a flat aromatic surface larger than that of the NDI core. This feature improves π-stacking interaction, thus implementing binding and affinity to the G4.[41] Stabilization of AR G4s by **7** was also corroborated by CD thermal unfolding analysis and *Taq* polymerase stop assay. Interestingly **6**, the other core-extended NDI, lacking the fourth condensed benzene, reported extremely reduce activity, highlighting the crucial role of that benzene ring in stabilizing the AR G4s.

At the cellular level, **7** exerted a greater cytotoxic effect in AR-positive than in AR-negative CRPC cells. Of note, the up-regulation of constitutively active AR-Vs has been implicated in AR-driven

tumor progression in CRPC.[57] In this context, as 22Rv1 cells express both AR-FL and AR-Vs, which in turn are remarkably down-regulated at mRNA and protein level upon NDI exposure, the superior antiproliferative activity observed in these cells compared to CRPC cells (e.g., DU145 and PC-3) that do not express the AR at all, could stem from a biological mechanism likely reflecting an AR addiction.[57]

Compound **7** was able to cause a marked decrease not only in the expression levels of AR but also of its main downstream regulated gene *KLK3* (PSA). In addition, transcriptomic analyses carried out in AR-positive *vs.* AR-negative cells after NDI exposure revealed remarkable changes also in the expression levels of genes known for their role in the onset and progression of cancer. In particular, we found a marked down-regulation of genes involved in different aspect of tumor cell biology, including cell cycle regulators (*CCND1*, *CCNE1*, *CDK4*, *CDKN2A*), apoptosis inhibitors (*BCL2*) and factors involved in Ras-MAP kinase signaling pathway (*KRAS*). Of note, a remarkable down-modulation in the expression of genes involved in signaling pathways (e.g., PI3K/AKT/mTOR and tyrosin kinase receptors) responsible for the persistent activation of AR program via feedback mechanisms[57] was also observed, among which we found *AKT1* and *ERBB2*.[57]

It has been reported that the levels of AKT1 mRNA and protein were significantly less in PCa cells transfected with a short hairpin RNA (shRNA) directed against AR3 than those in cells treated with a shRNA specific for the AR full length.[55] This evidence would suggest that the serine/threonine kinase AKT1 seems to be preferentially regulated by AR-Vs, as those expressed by 22Rv1 cells.[55,67]

In addition, we found that *PTEN* was up-regulated in 22Rv1 cells following the exposure to **7**. This evidence, along with the observed decrease in AKT1 mRNA levels and in the amounts of

basal and phoshorylated protein, suggests that exposure of 22Rv1 cells to NDI resulted in the shutdown of the PI3K/AKT/mTOR signaling pathway. Whether such an event is attributable to a direct or indirect effect of the NDI, via AR down-regulation, needs to be further investigated. Nonetheless, it is well documented that the deregulation of the AR acts concertedly with the aberrant activation of the PI3K/AKT/mTOR signaling axis in the progression towards the resistance to castration of PCa[60] as well as that the inhibition of AR or PI3K/AKT/mTOR alone results in a reciprocal feedback activation, thus contributing to the acquisition of ADT resistance.[68]

In this context, we observed that treatment of PCa cells with **7** in combination with the AR antagonist Enzalutamide resulted in a remarkable synergistic interaction in 22Rv1 but not in PC-3 cells. Importantly, **7**-treated 22Rv1 cells were characterized by a marked reduction in AR protein amounts (both AR-FL and AR-Vs), increased expression levels of PTEN and reduced AKT1 protein abundance. Conversely, PC-3 cells do not express AR or AR-Vs, lack PTEN expression and, upon exposure to NDI, are not characterized by a significant down-modulation of AKT1 (Figure 6E).

In keeping with these observations is the evidence that the exposure of PCa cells to Enzalutamide or Abiraterone acetate results in increased expression levels of AR-Vs but not of AR-full length,[56] suggesting that the adaptive shift towards the AR-Vs may contribute to the resistance of CRPC to second-generation drugs used in the ADT, as well as that a PCa subline selected *in vitro* for the resistance to Enzalutamide was characterized by decreased expression of AR and increased AKT activity.[68]

Moreover, it has been recently reported that Enzalutamide synergistically interacts with different pharmacological inhibitors of the PI3K/AKT/mTOR pathway, including BKM120, TKI258 and RAD001 in CRPC cells,[60] thus indicating that the concomitant inhibition of the AR and

PI3K/AKT/mTOR signaling pathway (as observed in NDI-treated 22Rv1 cells) may contribute to enhance the response of CRPC cells to AR signaling inhibitors.

In addition, we observed that exposure of 22Rv1 cells to **7** resulted in a remarkable down-modulation of *CCND1* and *CCNE1* and in the up-modulation of the pro-apoptotic gene *BAX* as well as that Enzalutamide act synergistically with **7** in 22Rv1 cells but not in PC-3 cells, where the compound induced the down-modulation of *BAX* and did not significantly affect the expression levels of the cell cycle regulators (Table S2 and Figure 6E). In keeping with our findings is the evidence that dihydrotestosterone-like compounds may enhance progression of PCa by increasing the transcriptional levels of cyclin D1 and E and reducing the expression levels of BAX.[69] In addition, it has been reported that *CCND1* is markedly up-regulated in circulating tumor cells from abiraterone/enzalutamide unresponsive *vs.* responsive PCa patients[61] as well as that RNAi-mediated depletion of CCND1 in ADT-resistant PCa cells results in the enhancement of Enzalutamide activity, thus indicating the Cyclin D is a determinant of the resistance of CRPC cells to ADT.[61]

In conclusion, although the effects of the tested NDI may not be limited to the repression of AR transcriptional activity but could involve additional G4 targets[70] our findings provide the rationale for the future development of alternative "third-line ADT" for CRPC. Moreover, as AR signaling plays a pivotal role in the development and progression of different malignancies, G4-based AR inhibitors could be also used in the future to treat other tumor types, including hormone-responsive cancer (e.g., breast cancer) as well as "non-hormonally" driven tumors, such as pancreatic cancer and hepatocellular carcinomas.[62]

EXPERIMENTAL SECTION

Materials and General Procedures. Reagents, oligonucleotides (TableS1), solvents and chemicals were purchased from Sigma-Aldrich (Milan, Italy) or TCI (Milan, Italy) and were used as supplied without further purification. HPLC analysis and purifications were performed using two different HPLC: Agilent system 1260 infinity, a Diode array detector and Fraction Collector III (for preparative) and an Agilent system SERIES 1260 (for analytical). The analytical column was XSelect HSS C18 2.5 μm (150 x 4.6 mm) (Waters, Milan, Italy). The preparative column was XSelect CSH Prep c18 5μm (150 x 30 mm) (Waters, Milan, Italy). Flows were 1.4 mL/min for analytical and 30 mL/min for preparative. For the analytical analysis were used the following method A: (Aqueous solvent: 0.1% trifluoroacetic acid in water; Organic solvent: Acetonitrile); Method A= 1.4 mL/min, Isocratic flow over 2 min 95% of aqueous solvent; gradient: 95% aqueous, gradually to 40% aqueous over 12 min and at the end an isocratic flow over 4 min. For the preparative purification was used the following method B: (Aqueous solvent: 0.1% trifluoroacetic acid in water; Organic solvent: Acetonitrile); Method B= 30 mL/min, Isocratic flow over 4 min 95% of aqueous solvent; gradient: 95% aqueous, gradually to 70% aqueous over 16 min and at the end an isocratic flow over 4 min). All the compounds purified have been tested in analytical HPLC (Method A) in order to determine their purity (≥95%). ^{1}H-, ^{13}C-NMR spectra were recorded on a Bruker ADVANCE 300 MHz spectrometer.

Synthesis and characterization. Synthesis of NDI 11: Reactant 10 (0.5 mmol) was dissolved into 40 mL of acetonitrile in a round bottom flask together with 1.5 mmol of 1,4-diaminobutane, the mixture was stirred at 75 °C for 4.5 h under argon. The resulting red solution was concentrated under vacuum and a red solid was obtained. The crude product was analysed by HPLC chromatography, (CH_3CN:H_2O 0.1%TFA) according to analytical method A and purified according to preparative method B, afforded the NDI **11** (yield 80%).

NDI: **11**·3CF_3COOH: Red solid; m.p. dec. > 200 °C. 1H-NMR (300 MHz, D_2O): 8.0.7 (d, J=8.0, 2H), 7.84 (d, J=8.0, 2H), 7.63 (s, 2H), 4.05-3.97 (m, 4H), 3.45 (bs, 2H), 3.20-3.11 (m, 4H), 3.02 (bs, 2H), 2.83 (s, 12H); 2.10-1.97 (m, 4H); 1.78 (bs, 4H). 13C-NMR (75 MHz, D_2O): 168.6; 167.1; 166.8; 166.5; 155.1; 134.1; 131.7; 130.0; 128.3; 127.4; 125.2; 123.2; 121.6; 101.7; 58.6; 58.5; 46.1; 45.6; 42.4; 41.1; 40.4; 29.1; 27.7; 26.1. Elemental analysis calcd (%) for $C_{34}H_{41}F_9N_6O_{10}$: C, 47.23; H, 4.78; F, 19.77; N, 9.72; O, 18.50. Found: C, 47.17; H, 4.79; N, 9.71.

Nucleophilic Aromatic Substitution: the NDI monomer (**11** or **12**, 0.25 mmol) was dissolved into 50 mL of acetonitrile in a round bottom flask together with 0.35 mmol of **10**, the mixture was stirred at 85 °C for 24 h under argon. The reaction mixture was cooled to room temperature to induce the precipitation of the crude product. The solid mixture was diluted in water, with 0.1% of TFA and purified by preparative HPLC chromatography, (CH_3CN:H_2O 0.1%TFA) according to preparative method B, obtaining the NDI dyads **8** (yield 51%) and **9** (yield 48%).

NDI: **8**·4CF_3COOH: Red solid; m.p. dec. > 200 °C. 1H-NMR (300 MHz, D_2O): 8.15 (d, J=7.96, 2H), 7.87 (d, J=7.96, 2H), 7.75 (s, 2H), 4.08-4.02 (m, 8H), 3.67 (bs, 4H), 3.16 (t, J=7.8, 8H), 2.83 (s, 24H); 2.08-2.01 (m, 12H). 13C-NMR (75 MHz, D_2O): 165.4; 163.7; 163.5; 163.1; 151.8; 130.7; 128.4; 126.1; 124.7; 124.3; 121.6; 120.4; 118.1; 98.4; 55.0; 42.6; 42.0; 37.4; 36.8; 30.1; 22.7; 22.6. Elemental analysis calcd (%) for $C_{60}H_{68}F_{12}N_{10}O_{16}$: C, 50.99; H, 4.85; F, 16.13; N, 9.91; O, 18.11. Found: C, 51.05; H, 4.86; N, 9.93.

NDI: **9**·4CF_3COOH: Red solid; m.p. dec. > 200 °C. 1H-NMR (300 MHz, D_2O): 8.05-8.02 (m, 2H), 7.80-7.77 (m, 4H), 4.07 (bs, 8H), 3.50 (bs, 4H), 3.26-3.18 (m, 8H), 2.88 (s, 24H); 2.12-2.05 (m, 8H); 1.88 (bs, 4H); 1.70 (bs, 6H). 13C-NMR (75 MHz, D_2O): 165.2; 163.7;163.4; 163.1; 151.8; 130.6; 128.3; 126.5; 124.8; 124.0; 121.6; 119.8; 118.0; 98.0; 55.2; 42.7; 37.6; 37.0; 25.5;

22.7; 22.6. Elemental analysis calcd (%) for $C_{63}H_{74}F_{12}N_{10}O_{16}$: C, 51.99; H, 5.13; F, 15.67; N, 9.62; O, 17.59. Found: C, 52.02; H, 5.10; N, 9.62.

Spectroscopic analyses (FRET and CD). For fluorescence melting curves, the 6-carboxyfluorescein (FAM) 5'-end- and 6-carboxy-tetramethylrhodamine (TAMRA) 3'-end labeled oligonucleotides (0.25 μM) (TableS1) were folded in lithium cacodylate buffer (10 mM, pH 7.4) and KCl 100 mM by heating at 95 °C for 5 min and gradually cooling to room temperature for 4 h. Where indicated, NDI derivates were added at the final concentration of 1 μM and, after additional 16 h at room temperature, samples were processed in a LightCycler 480 II (Roche, Milan, Italy). Oligonucleotide melting was monitored by observing FAM emission in the temperature range of 30-95 °C with 1 °C/min gradient. Melting profiles were normalized as previously described,[71] setting the initial value to 0 and the finale value to 1, and $T_{1/2}$ was defined as the temperature corresponding to the 0.5 fraction of the normalized fluorescence. For compound **7**, we also calculated T_m, as the minimum of the first derivative curve.

For CD analysis, oligonucleotides (Table S1) were diluted to a final concentration (4 μM) in lithium cacodylate buffer (10 mM, pH 7.4) and KCl 100 mM. Samples were annealed by heating at 95 °C for 5 min and were left cooling down at room temperature for 4 h. No temperature controller was employed. Where indicated, **7** was added at the final concentration of 16 μM, ad samples were incubated at room temperature for additional 16 h. For dsDNA, equimolar amounts of ssDNA and its complementary sequence (ssDNA compl, Table S1) were annealed. CD spectra were recorded on a Chirascan-Plus (Applied Photophysisics, Leatherhead, United Kingdom) equipped with a Peltier temperature controller using a quartz cell of 5 mm optical path length, over a wavelength range of 230-320 nm. The reported spectrum of each sample represents the average of 2 scans at 20 °C and it is baseline corrected for signal contributions due to the buffer. Observed

ellipticities were converted to mean residue ellipticity (θ) = deg×cm^2×dmol^{-1} (mol. ellip.). For the determination of T_m, spectra were recorded over a temperature range of 20-90 °C, with temperature increase of 5 °C. T_m values were calculated according to Greenfield.[72]

***Taq* polymerase stop assay.** AR Taq primer was 5'-end labeled with [γ-^{32}P]ATP using T4 polynucleotide kinase (Fermentas, Waltman, Massachusetts, United States) at 37 °C for 30 min. The labeled primer (final concentration 72 nM) was annealed to the template (final concentration 36 nM) (TableS1) in lithium cacodylate buffer (10 mM, pH 7.4) in the presence or absence of KCl 10 mM by heating at 95 °C for 5 min and gradually cooling to room temperature. Where specified, samples were incubated with 7 (12.5-200.0 nM), and primer extension was performed with 2 U/reaction of AmpliTaq Gold DNA polymerase (Applied Biosystem, Carlsbad, California, United States) at 60 °C for 30 min. Reactions were stopped by ethanol precipitation and primer extension products were separated on a 16 % denaturing gel, and finally visualized by phosphorimaging (Typhoon FLA 9000, GE Healthcare, Milan, Italy).

Surface Plasmon Resonance (SPR) analysis. SPR was performed on the Biacore T100 platform (GE Healthcare, Milan, Italy). 5'-biotinylated AR1 oligonucleotide was heated at 95 °C for 5 min and cooled down at room temperature to allow G4 folding in the presence of 10 mM Lithium Cacodilate and 150 mM KCl; 5'-biotinylated ssDNA was used as non-G4 negative control (TableS1). Immobilization was performed in HEPES-KCl running buffer (0.01 M HEPES pH 7.4, 0.15 M KCl, 3 mM EDTA) on a steptavidin coated surface (SA sensor chip, Biacore, GE Healthcare, Milan, Italy). Oligonucleotides were diluted in HEPES-KCl running buffer to a concentration of 30 nM and injected to reach the response of around 600 RU. Flow cell 1 was left empty to allow reference subtraction. Compounds binding analysis were performed at a flow rate of 40 μL/min, with contact time of 260 s and dissociation time of 600 s in HEPES-KCl buffer at

40 °C. Sensorgrams were obtained in the concentration range of 0.7-400 nM. After each compound injection the chip surface was regenerated twice with glycine 10 mM pH 2.0 solution (GE Healthcare, Milan, Italy). All sensorgrams were corrected by buffer injection response. Data were fitted to the Affinity – Steady State model using BIAevaluation software (GE Healthcare, Milan, Italy), measuring RU response 10 sec before the end of the association phase. All experiments were performed independently at least twice, and in each instance χ^2 values, which indicate the goodness of fitting, were below 5.3.

Cell lines and culture conditions. Human DU145 (HTB-81™), PC-3 (CRL-1435™), LNCaP (CRL-1740^{TM}) and 22Rv1 (CRL-2505™) prostate cancer cell lines were obtained from the American Type Culture Collection (ATCC, Rockville, Maryland, United states), whereas the human normal prostate cell line (PNT1A) was from Sigma-Aldrich (Milan, Italy). Cells were maintained as a monolayer in the logarithmic growth phase in Roswell Park Memorial Institute (RPMI)-1640 medium (Lonza Milan S.r.l, Treviglio, Italy) supplemented with 10% fetal calf serum at 37 °C in a humidified incubator at 5% CO_2. Cells were periodically monitored for DNA profile by short tandem repeats analysis using the AmpFISTR Identifiler PCR amplification kit (Thermo Fisher Scientific, Monza, Italy).

Assessment of NDI cytotoxic activity. For the assessment of the cytotoxic activity all the compounds were dissolved in dimethylsulfoxide (DMSO), stored at -20 °C and diluted in culture medium at the appropriate working concentrations immediately before use. The cytotoxic activity of the compounds was assessed after a 48-h of drug exposure by MTS (3-(4,5-dimethylthiazol-2-yl)-5-(3-carboxymethoxyphenyl)-2-(4-sulfophenyl)-2H-tetrazolium) assay (CellTiter 96® AQueous One Solution Cell Proliferation Assay, Promega Italia, Milan, Italy). Briefly, a suitable number of cell/well was seeded at in 96-well plates. After 24 h incubation at 37 °C, 5 % CO_2, cells

were treated with increasing concentrations (0.0001, 0.001, 0.01, 0.1, 1 and10 μM) of freshly diluted NDIs and incubated for 48 h. The number of viable cells was subsequently determined by incubating the cells for 4 h at 37 °C in the presence of 20 μL of MTS solution and by recording the absorbance at 490 nm, according to the manufacturer's instruction. The IC_{50} (concentration of ligand leading to 50% inhibition of cell viability) values were calculated from the dose-response curves (percentage inhibition of cell viability with respect to cells exposed to solvent (DMSO) as a function of the Log_{10} of NDI concentrations) using GraphPad Prism® 5.01 (GraphPad Software Inc., San Diego, California, United States).

For combination studies, the drugs were combined at fixed ratio in five concentrations (0.001 to 0.1 μM for **7** and 0.5 to 50 μM for Enzalutamide/MDV3100; Selleckchem, Houston, TX). Cells were incubated for 72 h at 37°C, 5% CO_2, and the cytotoxic activity subsequently assayed as described above. The type of pharmacological interaction was assessed by calculating the combination index (CI) at doses effecting 50% and 75% reduction in cell viability (ED_{50} and ED_{75}, respectively), according to Chou and Talalay's method using the Calcusyn program.[73] A CI < 1 reflects a synergistic interaction; CI = 1 indicates an additive effect; CI > 1 evidences antagonism.

Gene expression analysis and assessment of telomerase activity. Total RNA was isolated from cultured cells using the Qiagen RNeasy Mini kit (Qiagen, Hilden, Germany) and digested with 20 U RNase-free DNase. Total RNA (0.5 μg) was randomly primed and reverse transcribed using the High Capacity cDNA Reverse Transcription kit (Applied Biosystems, Foster City, California, USA). The quantification of AR and KLK3 mRNA expression levels was assessed by TaqMan® Assay (Hs00907244_m1 and Hs02576345_m1, respectively; Applied Biosystems, Carlsbad, California, United States) using the 7900HT Fast Real-Time PCR System. Data were analyzed by SDS 2.2.2 software and, if not otherwise specified, reported as relative quantity (RQ)

with respect to untreated cells (calibrator sample), according to the $2^{\wedge-\Delta\Delta Ct}$ method,[74] where Ct represents the threshold cycle. RNaseP (TaqMan® RNase P Control Reagents) was used as housekeeping gene (normalizer sample).

The expression levels of 92 genes associated with the molecular mechanisms of cancer were assessed using TaqMan® Arrays (PN4418806; Applied Biosystems, Carlsbad, California, United States). Modulation of gene expression in treated compared to untreated cells was assessed by the $2^{-\Delta\Delta Ct}$ method, as described above. The average expression levels of 4 housekeeping genes (*18S*, *GAPDH*, *HPRT1* and *GUSB*) present in each array were used as normalizer.

Telomerase activity was measured on 1 μg of proteins by the radioactive (^{32}P) telomeric-repeat amplification protocol (TRAP) using the TRAPeze kit (Merck S.p.A., Vimodrone, Italy), according to the manufacturer's protocol. Each reaction product was amplified in the presence of a 36-bp internal TRAP assay standard. A TSR8 quantification standard (which serves as a standard to estimate the amount of product extended by telomerase in a given protein extract) was included for each set of TRAP assays. PCR amplification products were then resolved by polyacrylamide gel electrophoresis and visualized by autoradiography. Quantitative analysis was performed upon densitometric evaluation of the digital image by ImageJ 1.46r. Relative telomerase activity was then calculated as reported by Folini et al.[75]

Western immunoblotting. Total protein extracts were prepared according to standard methods. Forty μg of protein extracts were fractioned by SDS-PAGE and transferred onto Hybond nitrocellulose filters (RPN 303D, GE Healthcare, Milan, Italy). Filters were blocked in PBS-Tween 20, 5% skim milk and incubated overnight with the following primary antibodies: rabbit polyclonal raised against AR (PG-21, cat # 06-680, Merck S.p.a., Vimodrone, Italy); rabbit

monoclonal raised against PSA/KLK3 (D2A8) (#5877, Cell Signaling Technology, Danvers, MA); rabbit polyclonal raised against Cyclin D1 (H-295) (sc-753, Santa Cruz Biotechnology, Dallas, TX); mouse monoclonal raised against AKT1 (#610861, Becton Dickinson Italia, Milano, Italy). Mouse monoclonal anti Vinculin (VCL, V9131, Sigma-Aldrich S.r.l., Milan, Italy) or β-actin (ACTB) antibody (ab8226, Abcam, Cambridge, United Kingdom) were used to ensure equal protein loading. The filters were then probed with secondary peroxidase-linked whole antibodies (GE Healthcare, Milan, Italy) and detected by Novex® ECL HRP Chemiluminescent detection system (Thermo Fisher Scientific, Monza, Italy). Filters were then subjected to autoradiography, scanned (ImageScanner III, GE Healthcare, Milan, Italy) and analysed using ImageJ 1.46r.

ASSOCIATED CONTENT

Supporting Information.

The file includes:
- Supplementary methods:
  - Analysis of compound **7** cellular internalization.
- Supplementary tables:
  - **Table S1.** Oligonucleotides used in this study.
  - **Table S2.** Analysis of gene expression levels in 22Rv1, PC-3 and DU145 cells upon a 48-h exposure to NDI (IC_{50}).
- Supplementary figures:
  - **Figure S1.** FRET-melting curves of AR1 and AR3 G4s.
  - **Figure S2.** Biological effects of NDIs on CRPC cells.
  - **Figure S3.** CD analysis of ssDNA and dsDNA controls.
  - **Figure S4.** SPR analysis raw data and data fitting for the binding of all compounds toward AR1 G4.
  - HPLC Purity data.
  - ^{1}H- and ^{13}C-NMR spectra of the compounds **11**, **8** and **9.**

Molecular formula strings are available.

AUTHOR INFORMATION

Corresponding Author

* For M. Folini: phone, +39 02 2390 5027; fax, +39 02 2390 2692;

E-mail, marco.folini@istitutotumori.mi.it

* For S.N. Richter: phone, +39 049 8272346; fax, +39 049 8272355;

E-mail, sara.richter@unipd.it

Author Contributions

The manuscript was written through contributions of all authors. All authors have given approval to the final version of the manuscript. ‡These authors contributed equally.

ACKNOWLEDGMENT

This work was supported by grants from European Research Council (ERC Consolidator grant 615879 to S.N. Richter) and by Fondazione I. Monzino (grant to M. Folini). The authors are thankful to Dr. P. Casalini (Microscopy facility, Fondazione IRCCS Istituto Nazionale dei Tumori di Milano) for her helpful support in cell imaging analyses.

ABBREVIATIONS

ADT, androgen deprivation therapy; AR, androgen receptor; CD, circular dichroism; CRCP, castration resistant prostate cancer; FRET, Fluorescence Resonance Energy Transfer; G4, G-quadruplex; mCRPC, metastatic castration resistant prostate cancer; NDIs, naphthalene diimides; PCa, prostate cancer; SPR, surface plasmon resonance.

REFERENCES

(1) Watson, P. A.; Arora, V. K.; Sawyers, C. L. Emerging Mechanisms of Resistance to Androgen Receptor Inhibitors in Prostate Cancer. *Nat. Rev. Cancer* **2015**, *15* (12), 701–711.

(2) Crona, D. J.; Whang, Y. E. Androgen Receptor-Dependent and -Independent Mechanisms Involved in Prostate Cancer Therapy Resistance. *Cancers (Basel).* **2017**, *9* (6), 67.

(3) Baldari, S.; Boni, G.; Bortolus, R.; Caffo, O.; Conti, G.; De Vincentis, G.; Monari, F.; Procopio, G.; Santini, D.; Seregni, E.; Valdagni, R.. Management of Metastatic Castration-Resistant Prostate Cancer: A Focus on Radium-223: Opinions and Suggestions from an Expert Multidisciplinary Panel. *Crit. Rev. Oncol. Hematol.* **2017**, *113*, 43–51.

(4) Ceder, Y.; Bjartell, A.; Culig, Z.; Rubin, M. A.; Tomlins, S.; Visakorpi, T. The Molecular Evolution of Castration-Resistant Prostate Cancer. *Eur. Urol. Focus* **2016**, *2* (5), 506–513.

(5) Shore, N.; Heidenreich, A.; Saad, F. Predicting Response and Recognizing Resistance: Improving Outcomes in Patients With Castration-Resistant Prostate Cancer. *Urology* **2017**, *109*, 6–18.

(6) Mitchell, T.; Ramos-Montoya, A.; Di Antonio, M.; Murat, P.; Ohnmacht, S.; Micco, M.; Jurmeister, S.; Fryer, L.; Balasubramanian, S.; Neidle, S.; Neal, D.E. Downregulation of Androgen Receptor Transcription by Promoter G-Quadruplex Stabilization as a Potential Alternative Treatment for Castrate-Resistant Prostate Cancer. *Biochemistry* **2013**, *52* (8), 1429–1436.

(7) Lipps, H. J.; Rhodes, D. G-Quadruplex Structures: In Vivo Evidence and Function. *Trends Cell Biol.* **2009**, *19* (8), 414–422.

(8) Campbell, N. H.; Neidle, S. G-Quadruplexes and Metal Ions. *Met. Ions Life Sci.* **2012**, *10*,

119–134.

(9) Du, Z.; Zhao, Y.; Li, N. Genome-Wide Analysis Reveals Regulatory Role of G4 DNA in Gene Transcription. *Genome Res.* **2008**, *18* (2), 233–241.

(10) Hershman, S. G.; Chen, Q.; Lee, J. Y.; Kozak, M. L.; Yue, P.; Wang, L.-S.; Johnson, F. B. Genomic Distribution and Functional Analyses of Potential G-Quadruplex-Forming Sequences in Saccharomyces Cerevisiae. *Nucleic Acids Res.* **2008**, *36* (1), 144–156.

(11) Perrone, R.; Lavezzo, E.; Riello, E.; Manganelli, R.; Palù, G.; Toppo, S.; Provvedi, R.; Richter, S. N. Mapping and Characterization of G-Quadruplexes in Mycobacterium Tuberculosis Gene Promoter Regions. *Sci. Rep.* **2017**, *7* (1), 5743.

(12) Beaume, N.; Pathak, R.; Yadav, V. K.; Kota, S.; Misra, H. S.; Gautam, H. K.; Chowdhury, S. Genome-Wide Study Predicts Promoter-G4 DNA Motifs Regulate Selective Functions in Bacteria: Radioresistance of D. Radiodurans Involves G4 DNA-Mediated Regulation. *Nucleic Acids Res.* **2013**, *41* (1), 76–89.

(13) Rawal, P.; Kummarasetti, V. B. R.; Ravindran, J.; Kumar, N.; Halder, K.; Sharma, R.; Mukerji, M.; Das, S. K.; Chowdhury, S. Genome-Wide Prediction of G4 DNA as Regulatory Motifs: Role in Escherichia Coli Global Regulation. *Genome Res.* **2006**, *16* (5), 644–655.

(14) Wieland, M.; Hartig, J. S. Investigation of mRNA Quadruplex Formation in Escherichia Coli. *Nat. Protoc.* **2009**, *4* (11), 1632–1640.

(15) Thakur, R. S.; Desingu, A.; Basavaraju, S.; Subramanya, S.; Rao, D. N.; Nagaraju, G. Mycobacterium Tuberculosis DinG Is a Structure-Specific Helicase That Unwinds G4

DNA: Implications for Targeting G4 DNA as a Novel Therapeutic Approach. *J. Biol. Chem.* **2014**, *289* (36), 25112–25136.

(16) Shukla, K.; Thakur, R. S.; Ganguli, D.; Rao, D. N.; Nagaraju, G. Escherichia ColiandNeisseria gonorrhoeaeUvrD Helicase Unwinds G4 DNA Structures. *Biochem. J.* **2017**, *474* (21), 3579–3597.

(17) Perrone, R.; Nadai, M.; Poe, J. A.; Frasson, I.; Palumbo, M.; Palù, G.; Smithgall, T. E.; Richter, S. N. Formation of a Unique Cluster of G-Quadruplex Structures in the HIV-1 Nef Coding Region: Implications for Antiviral Activity. *PLoS One* **2013**, *8* (8), e73121.

(18) Perrone, R.; Nadai, M.; Frasson, I.; Poe, J. A.; Butovskaya, E.; Smithgall, T. E.; Palumbo, M.; Palù, G.; Richter, S. N. A Dynamic G-Quadruplex Region Regulates the HIV-1 Long Terminal Repeat Promoter. *J. Med. Chem.* **2013**, *56* (16), 6521–6530.

(19) Ruggiero, E.; Richter, S. N. G-Quadruplexes and G-Quadruplex Ligands: Targets and Tools in Antiviral Therapy. *Nucleic Acids Res.* **2018**.

(20) Rhodes, D.; Lipps, H. J. G-Quadruplexes and Their Regulatory Roles in Biology. *Nucleic Acids Res.* **2015**, *43* (18), 8627–8637.

(21) Holder, I. T.; Hartig, J. S. A Matter of Location: Influence of G-Quadruplexes on Escherichia Coli Gene Expression. *Chem. Biol.* **2014**, *21* (11), 1511–1521.

(22) Zhou, B.; Liu, C.; Geng, Y.; Zhu, G. Topology of a G-Quadruplex DNA Formed by C9orf72 Hexanucleotide Repeats Associated with ALS and FTD. *Sci. Rep.* **2015**, *5* (1), 16673.

(23) Maizels, N. G4-Associated Human Diseases. *EMBO Rep.* **2015**, *16* (8), 910–922.

(24) Murat, P.; Balasubramanian, S. Existence and Consequences of G-Quadruplex Structures in DNA. *Curr. Opin. Genet. Dev.* **2014**, *25*, 22–29.

(25) Biffi, G.; Tannahill, D.; McCafferty, J.; Balasubramanian, S. Quantitative Visualization of DNA G-Quadruplex Structures in Human Cells. *Nat. Chem.* **2013**, *5* (3), 182–186.

(26) Henderson, A.; Wu, Y.; Huang, Y. C.; Chavez, E. A.; Platt, J.; Johnson, F. B.; Brosh, R. M.; Sen, D.; Lansdorp, P. M. Detection of G-Quadruplex DNA in Mammalian Cells. *Nucleic Acids Res.* **2014**, *42* (2), 860–869.

(27) Tosoni, E.; Frasson, I.; Scalabrin, M.; Perrone, R.; Butovskaya, E.; Nadai, M.; Palù, G.; Fabris, D.; Richter, S. N. Nucleolin Stabilizes G-Quadruplex Structures Folded by the LTR Promoter and Silences HIV-1 Viral Transcription. *Nucleic Acids Res.* **2015**, *43* (18), 8884–8897.

(28) Scalabrin, M.; Frasson, I.; Ruggiero, E.; Perrone, R.; Tosoni, E.; Lago, S.; Tassinari, M.; Palù, G.; Richter, S. N. The Cellular Protein hnRNP A2/B1 Enhances HIV-1 Transcription by Unfolding LTR Promoter G-Quadruplexes. *Sci. Rep.* **2017**, *7*, 45244.

(29) Mendoza, O.; Bourdoncle, A.; Boulé, J.-B.; Brosh, R. M.; Mergny, J.-L. G-Quadruplexes and Helicases. *Nucleic Acids Res.* **2016**, *44* (5), 1989–2006.

(30) Shen, M. M.; Abate-Shen, C. Molecular Genetics of Prostate Cancer: New Prospects for Old Challenges. *Genes Dev.* **2010**, *24* (18), 1967–2000.

(31) Siddiqui-Jain, A.; Grand, C. L.; Bearss, D. J.; Hurley, L. H. Direct Evidence for a G-Quadruplex in a Promoter Region and Its Targeting with a Small Molecule to Repress c-MYC Transcription. *Proc. Natl. Acad. Sci.* **2002**, *99* (18), 11593–11598.

(32) Leonetti, C.; Amodei, S.; D'Angelo, C.; Rizzo, A.; Benassi, B.; Antonelli, A.; Elli, R.; Stevens, M. F. G.; D'Incalci, M.; Zupi, G.; Biroccio, A. Biological Activity of the G-Quadruplex Ligand RHPS4 (3,11-Difluoro-6,8,13-Trimethyl-8H-quino[4,3,2-Kl]acridinium Methosulfate) Is Associated with Telomere Capping Alteration. *Mol. Pharmacol.* **2004**, *66* (5), 1138–1146.

(33) Balasubramanian, S.; Hurley, L. H.; Neidle, S. Targeting G-Quadruplexes in Gene Promoters: A Novel Anticancer Strategy? *Nat. Rev. Drug Discov.* **2011**, *10* (4), 261–275.

(34) Ali, A.; Bhattacharya, S. DNA Binders in Clinical Trials and Chemotherapy. *Bioorg. Med. Chem.* **2014**, *22* (16), 4506–4521.

(35) Rodriguez, R.; Miller, K. M.; Forment, J. V; Bradshaw, C. R.; Nikan, M.; Britton, S.; Oelschlaegel, T.; Xhemalce, B.; Balasubramanian, S.; Jackson, S. P. Small-Molecule-Induced DNA Damage Identifies Alternative DNA Structures in Human Genes. *Nat. Chem. Biol.* **2012**, *8* (3), 301–310.

(36) Collie, G. W.; Promontorio, R.; Hampel, S. M.; Micco, M.; Neidle, S.; Parkinson, G. N. Structural Basis for Telomeric G-Quadruplex Targeting by Naphthalene Diimide Ligands. *J. Am. Chem. Soc.* **2012**, *134* (5), 2723–2731.

(37) Micco, M.; Collie, G. W.; Dale, A. G.; Ohnmacht, S. A.; Pazitna, I.; Gunaratnam, M.; Reszka, A. P.; Neidle, S. Structure-Based Design and Evaluation of Naphthalene Diimide G-Quadruplex Ligands as Telomere Targeting Agents in Pancreatic Cancer Cells. *J. Med. Chem.* **2013**, *56* (7), 2959–2974.

(38) Doria, F.; Nadai, M.; Sattin, G.; Pasotti, L.; Richter, S. N.; Freccero, M. Water Soluble

Extended Naphthalene Diimides as pH Fluorescent Sensors and G-Quadruplex Ligands. *Org. Biomol. Chem.* **2012**, *10* (19), 3830–3840.

(39) Nadai, M.; Doria, F.; Di Antonio, M.; Sattin, G.; Germani, L.; Percivalle, C.; Palumbo, M.; Richter, S. N.; Freccero, M. Naphthalene Diimide Scaffolds with Dual Reversible and Covalent Interaction Properties towards G-Quadruplex. *Biochimie* **2011**, *93* (8), 1328–1340.

(40) Nadai, M.; Doria, F.; Germani, L.; Richter, S. N.; Freccero, M. A Photoreactive G-Quadruplex Ligand Triggered by Green Light. *Chemistry* **2015**, *21* (6), 2330–2334.

(41) Perrone, R.; Doria, F.; Butovskaya, E.; Frasson, I.; Botti, S.; Scalabrin, M.; Lago, S.; Grande, V.; Nadai, M.; Freccero, M.; Richter, S. N.. Synthesis, Binding and Antiviral Properties of Potent Core-Extended Naphthalene Diimides Targeting the HIV-1 Long Terminal Repeat Promoter G-Quadruplexes. *J. Med. Chem.* **2015**, *58* (24), 9639–9652.

(42) Ohnmacht, S. A.; Marchetti, C.; Gunaratnam, M.; Besser, R. J.; Haider, S. M.; Di Vita, G.; Lowe, H. L.; Mellinas-Gomez, M.; Diocou, S.; Robson, M.; Šponer, J.; Islam, B.; Pedley, R. B.; Hartley, J. A.; Neidle, S. A G-Quadruplex-Binding Compound Showing Anti-Tumour Activity in an in Vivo Model for Pancreatic Cancer. *Sci. Rep.* **2015**, *5* (1), 11385.

(43) Franceschin, M.; Rossetti, L.; D'Ambrosio, A.; Schirripa, S.; Bianco, A.; Ortaggi, G.; Savino, M.; Schultes, C.; Neidle, S. Natural and Synthetic G-Quadruplex Interactive Berberine Derivatives. *Bioorg. Med. Chem. Lett.* **2006**, *16* (6), 1707–1711.

(44) Kim, M.-Y.; Vankayalapati, H.; Shin-ya, K.; Wierzba, K.; Hurley, L. H. Telomestatin, a Potent Telomerase Inhibitor That Interacts Quite Specifically with the Human Telomeric

Intramolecular G-Quadruplex. *J. Am. Chem. Soc.* **2002**, *124* (10), 2098–2099.

(45) Dai, J.; Carver, M.; Hurley, L. H.; Yang, D. Solution Structure of a 2:1 Quindoline-c-MYC G-Quadruplex: Insights into G-Quadruplex-Interactive Small Molecule Drug Design. *J. Am. Chem. Soc*. **2011**, *133* (44), 17673–17680.

(46) Doria, F.; Manet, I.; Grande, V.; Monti, S.; Freccero, M. Water-Soluble Naphthalene Diimides as Singlet Oxygen Sensitizers. *J. Org. Chem.* **2013**, *78* (16), 8065–8073.

(47) Nadai, M.; Cimino-Reale, G.; Sattin, G.; Doria, F.; Butovskaya, E.; Zaffaroni, N.; Freccero, M.; Palumbo, M.; Richter, S. N.; Folini, M. Assessment of Gene Promoter G-quadruplex Binding and Modulation by a Naphthalene Diimide Derivative in Tumor Cells. *Int. J. Oncol.* **2015**, *46* (1), 369–380.

(48) Doria, F.; Folini, M.; Grande, V.; Cimino-Reale, G.; Zaffaroni, N.; Freccero, M. Naphthalene Diimides as Red Fluorescent pH Sensors for Functional Cell Imaging. *Org. Biomol. Chem.* **2015**, *13* (2), 570–576.

(49) Doria, F.; Nadai, M.; Costa, G.; Sattin, G.; Gallati, C.; Bergamaschi, G.; Moraca, F.; Alcaro, S.; Freccero, M.; Richter, S. N. Extended Naphthalene Diimides with Donor/Acceptor Hydrogen-Bonding Properties Targeting G-Quadruplex Nucleic Acids. *European J. Org. Chem.* **2016**, *2016* (28), 4824–4833.

(50) Sampson, N.; Neuwirt, H.; Puhr, M.; Klocker, H.; Eder, I. E. In Vitro Model Systems to Study Androgen Receptor Signaling in Prostate Cancer. *Endocr. Relat. Cancer* **2013**, *20* (2), R49-64.

(51) Cunningham, D.; You, Z. In Vitro and in Vivo Model Systems Used in Prostate Cancer

Research. *J. Biol. Methods* **2015**, *2* (1), 17.

(52) Avancès, C.; Georget, V.; Térouanne, B.; Orio, F.; Cussenot, O.; Mottet, N.; Costa, P.; Sultan, C. Human Prostatic Cell Line PNT1A, a Useful Tool for Studying Androgen Receptor Transcriptional Activity and Its Differential Subnuclear Localization in the Presence of Androgens and Antiandrogens. *Mol. Cell. Endocrinol.* **2001**, *184* (1–2), 13–24.

(53) Mitchell, S.; Abel, P.; Ware, M.; Stamp, G.; Lalani, E. Phenotypic and Genotypic Characterization of Commonly Used Human Prostatic Cell Lines. *BJU Int.* **2000**, *85* (7), 932–944.

(54) Gray, R. D.; Chaires, J. B. Analysis of Multidimensional G-Quadruplex Melting Curves. *Curr. Protoc. nucleic acid Chem.* **2011**, *45* (1), 17.4.1-17.4.16

(55) Guo, Z.; Yang, X.; Sun, F.; Jiang, R.; Linn, D. E.; Chen, H.; Chen, H.; Kong, X.; Melamed, J.; Tepper, C. G.; Kung, H. J.; Brodie, A. M.; Edwards, J.; Qiu, Y. A Novel Androgen Receptor Splice Variant Is up-Regulated during Prostate Cancer Progression and Promotes Androgen Depletion-Resistant Growth. *Cancer Res.* **2009**, *69* (6), 2305–2313.

(56) Hu, R.; Lu, C.; Mostaghel, E. A.; Yegnasubramanian, S.; Gurel, M.; Tannahill, C.; Edwards, J.; Isaacs, W. B.; Nelson, P. S.; Bluemn, E.; Plymate, S. R.; Luo, J. Distinct Transcriptional Programs Mediated by the Ligand-Dependent Full-Length Androgen Receptor and Its Splice Variants in Castration-Resistant Prostate Cancer. *Cancer Res.* **2012**, *72* (14), 3457–3462.

(57) Schweizer, M. T.; Yu, E. Y. Persistent Androgen Receptor Addiction in Castration-Resistant Prostate Cancer. *J. Hematol. Oncol.* **2015**, *8*, 128.

(58) Bidzinska, J.; Cimino-Reale, G.; Zaffaroni, N.; Folini, M. G-Quadruplex Structures in the Human Genome as Novel Therapeutic Targets. *Molecules* **2013**, *18* (10), 12368–12395.

(59) Liu, S.; Qi, Y.; Ge, Y.; Duplessis, T.; Rowan, B. G.; Ip, C.; Cheng, H.; Rennie, P. S.; Horikawa, I.; Lustig, A. J.; Yu, Q.; Zhang, H.; Dong, Y. Telomerase as an Important Target of Androgen Signaling Blockade for Prostate Cancer Treatment. *Mol. Cancer Ther.* **2010**, *9* (7), 2016–2025.

(60) Yadav, S. S.; Li, J.; Stockert, J. A.; O'Connor, J.; Herzog, B.; Elaiho, C.; Galsky, M. D.; Tewari, A. K.; Yadav, K. K. Combination Effect of Therapies Targeting the PI3K- and AR-Signaling Pathways in Prostate Cancer. *Oncotarget* **2016**, *7* (46), 76181–76196.

(61) Pal, S. K.; Patel, J.; He, M.; Foulk, B.; Kraft, K.; Smirnov, D. A.; Twardowski, P.; Kortylewski, M.; Bhargava, V.; Jones, J. O. Identification of Mechanisms of Resistance to Treatment with Abiraterone Acetate or Enzalutamide in Patients with Castration-Resistant Prostate Cancer (CRPC). *Cancer* **2018**, *124* (6), 1216–1224.

(62) Schweizer, M.; Yu, E. AR-Signaling in Human Malignancies: Prostate Cancer and Beyond. *Cancers (Basel).* **2017**, *9* (1), 7.

(63) Lu, J.; Van der Steen, T.; Tindall, D. J. Are Androgen Receptor Variants a Substitute for the Full-Length Receptor? *Nat. Rev. Urol.* **2015**, *12* (3), 137–144.

(64) Barbieri, C. E.; Bangma, C. H.; Bjartell, A.; Catto, J. W. F.; Culig, Z.; Grönberg, H.; Luo, J.; Visakorpi, T.; Rubin, M. A. The Mutational Landscape of Prostate Cancer. *Eur. Urol.* **2013**, *64* (4), 567–576.

(65) Visakorpi, T.; Hyytinen, E.; Koivisto, P.; Tanner, M.; Keinänen, R.; Palmberg, C.; Palotie,

A.; Tammela, T.; Isola, J.; Kallioniemi, O. P. In Vivo Amplification of the Androgen Receptor Gene and Progression of Human Prostate Cancer. *Nat. Genet.* **1995**, *9* (4), 401–406.

(66) Taylor, B. S.; Schultz, N.; Hieronymus, H.; Gopalan, A.; Xiao, Y.; Carver, B. S.; Arora, V. K.; Kaushik, P.; Cerami, E.; Reva, B.; Antipin, Y.; Mitsiades, N.; Landers, T.; Dolgalev, I.; Major, J. E.; Wilson, M.; Socci, N. D.; Lash, A. E.; Heguy, A.; Eastham, J. A.; Scher, H. I.; Reuter, V. E.; Scardino, P. T.; Sander, C.; Sawyers, C. L.; Gerald, W. L. Integrative Genomic Profiling of Human Prostate Cancer. *Cancer Cell* **2010**, *18* (1), 11–22.

(67) Lu, J.; Van der Steen, T.; Tindall, D. J. Are Androgen Receptor Variants a Substitute for the Full-Length Receptor? *Nat. Rev. Urol.* **2015**, *12* (3), 137–144.

(68) Qi, W.; Morales, C.; Cooke, L. S.; Johnson, B.; Somer, B.; Mahadevan, D. Reciprocal Feedback Inhibition of the Androgen Receptor and PI3K as a Novel Therapy for Castrate-Sensitive and -Resistant Prostate Cancer. *Oncotarget* **2015**, *6* (39), 41976–41987.

(69) Kim, S. H.; Nam, K. H.; Hwang, K. A.; Choi, K. C. Influence of Hexabromocyclododecane and 4-Nonylphenol on the Regulation of Cell Growth, Apoptosis and Migration in Prostatic Cancer Cells. *Toxicol. Vitr.* **2016**, *32*, 240–247.

(70) Marchetti, C.; Zyner, K. G.; Ohnmacht, S. A.; Robson, M.; Haider, S. M.; Morton, J. P.; Marsico, G.; Vo, T.; Laughlin-Toth, S.; Ahmed, A. A.; Di Vita, G.; Pazitna, I.; Gunaratnam, M.; Besser, R. J.; Andrade, A. C.G.; Diocou, S.; Pike, J.A.; Tannahill, D.; Pedley, R.B.; Evans, T. R. J.; Wilson, W. D.; Balasubramanian, S.; Neidle, S. . Targeting Multiple Effector Pathways in Pancreatic Ductal Adenocarcinoma with a G-Quadruplex-Binding Small Molecule. *J. Med. Chem.* **2018**, *61* (6), 2500–2517.

(71) Rachwal, P. A.; Fox, K. R. Quadruplex Melting. *Methods* **2007**, *43* (4), 291–301.

(72) Greenfield, N. J. Using Circular Dichroism Collected as a Function of Temperature to Determine the Thermodynamics of Protein Unfolding and Binding Interactions. *Nat. Protoc.* **2007**, *1* (6), 2527–2535.

(73) Chou, T.-C. Preclinical versus Clinical Drug Combination Studies. *Leuk. Lymphoma* **2008**, *49* (11), 2059–2080.

(74) Livak, K. J.; Schmittgen, T. D. Analysis of Relative Gene Expression Data Using Real-Time Quantitative PCR and the 2(-Delta Delta C(T)) Method. *Methods* **2001**, *25* (4), 402–408.

(75) Folini, M.; Pivetta, C.; Zagotto, G.; De Marco, C.; Palumbo, M.; Zaffaroni, N.; Sissi, C. Remarkable Interference with Telomeric Function by a G-Quadruplex Selective Bisantrene Regioisomer. *Biochem. Pharmacol.* **2010**, *79* (12), 1781–1790.

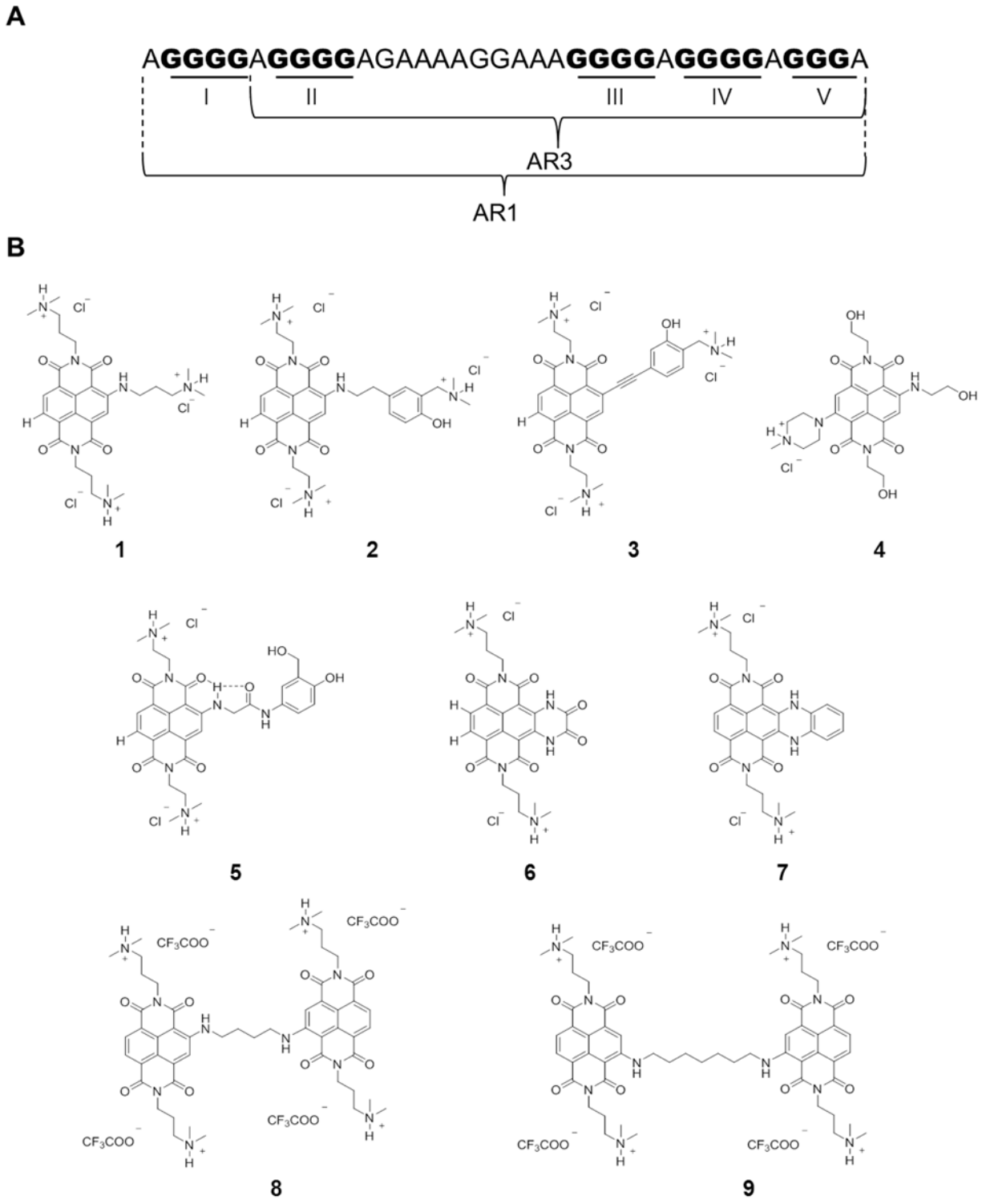

Figure 1. Target and ligands. (A) Nucleotide sequence of the AR promoter at -116 bases from the gene transcription start site. Several G4 conformations may form: G-tracts are in bold, underlined

and numbered (I-V). The two sequences that were characterized and investigated (AR1 and AR3) are shown. (B) NDI derivatives tested for their binding to AR G4s.

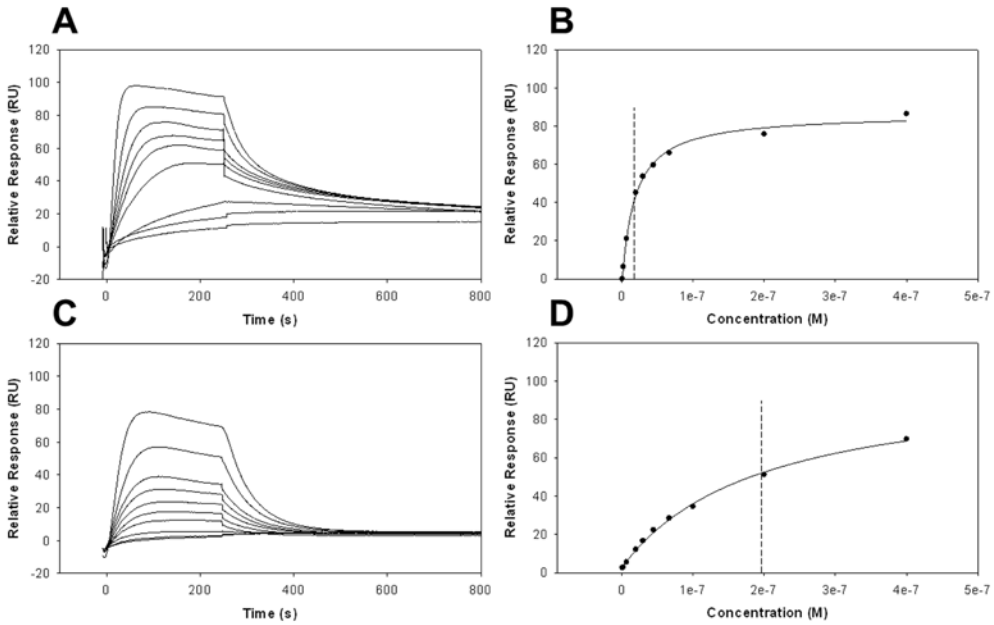

Figure 2. SPR analysis of **7** binding toward AR1 G4 (A and B) and ssDNA (C and D). Right panels represent data fitting according to the Steady state affinity model. Biosensor data were collected at 40 °C; the compound was injected at increasing concentrations (0.7-400 nM).

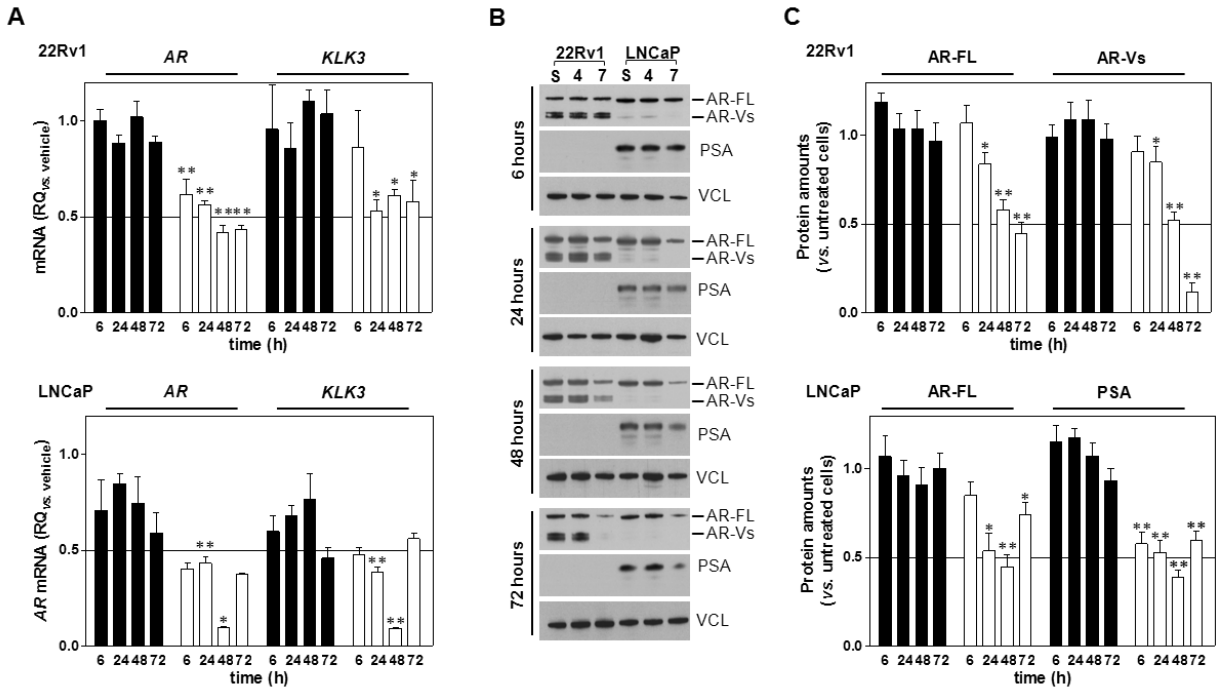

Figure 3. Exposure of AR-positive PCa cells to 7 results in the down-regulation of AR and PSA. (A) Real-time RT-PCR analysis of *AR* and *KLK3* mRNA expression levels over time in **4**- (black bars) and **7**-treated (white bars) 22Rv1 and LNCaP cells. Data have been reported as relative quantity (RQ) with respect to untreated cells (i.e., solvent (DMSO) exposure) at each time point, according to the $2^{\wedge\text{-}\Delta\Delta Ct}$ method, and represent mean values ± s.d. (B) Representative western immunoblotting showing AR and PSA protein amounts over time in untreated (S: solvent), **4**- and **7**-treated 22Rv1 and LNCaP cells. Vinculin (VCL) was used as loading control. Cropped images of selected proteins are shown. Full length (AR-FL) and variant (AR-Vs) forms of the androgen receptor are indicated. (C) Quantification of AR and PSA proteins Data have been reported as relative quantity (AR-FL, AR-Vs and PSA) in **4**- and **7**-treated *vs.* untreated (solvent) cells and represent mean values ± s.d. from at least three independent experiments. *$P < 0.05$; **$P < 0.01$ (Student's t-test).

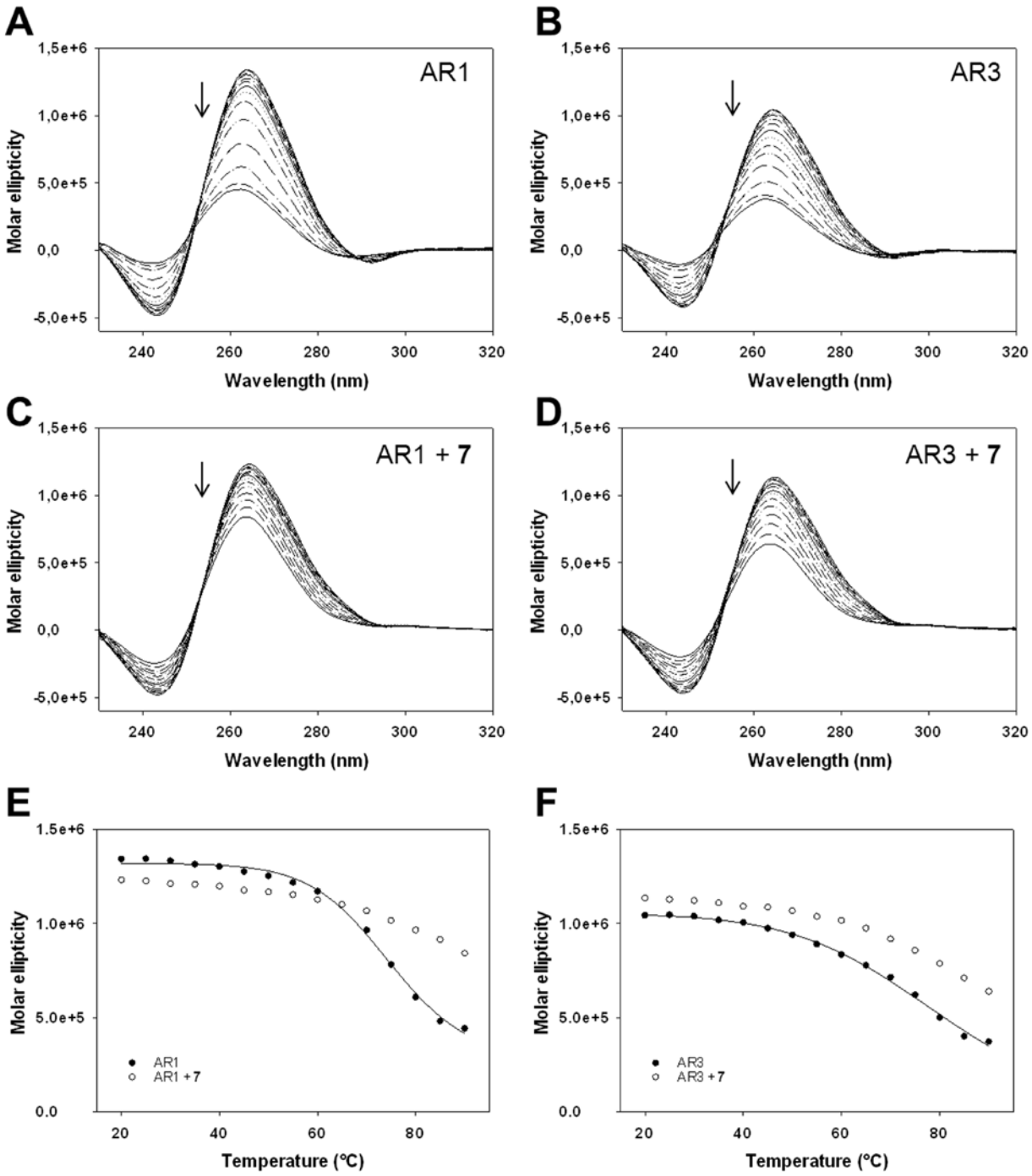

Figure 4. Representative CD analysis of AR1 and AR3 G4s (4 μM) at K^+ 100 mM in the presence of **7** (16 μM) (C and D) or the same amount of DMSO (A and B). CD spectra variation is shown as a function of the wavelength; arrows indicate the spectral change from 20 °C to 90 °C. The

molar ellipticity of AR1 (E) and AR3 (F) at the peak wavelengths is shown as a function of the temperature. Each thermal unfolding analysis was performed twice.

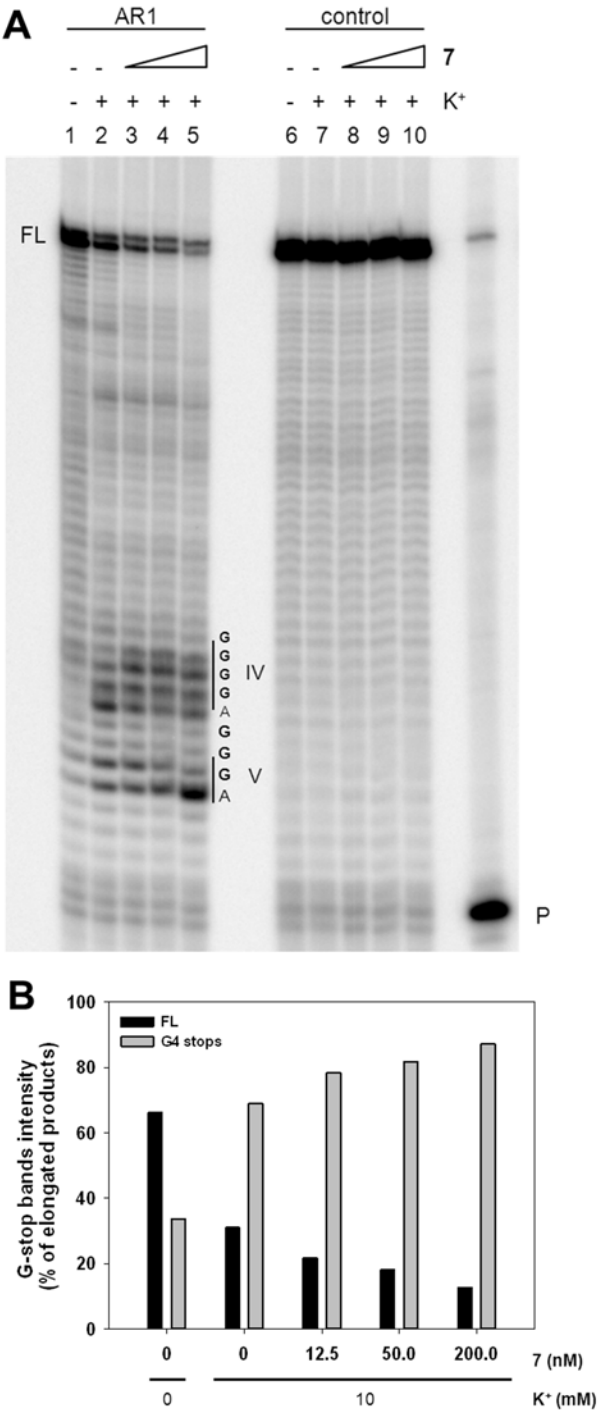

Figure 5. (A) Image of a typical *Taq* polymerase stop assay. The AR1 template was amplified by *Taq* polymerase in the absence (lane 1) and in the presence of 10 mM K^+, combined with increasing

amounts (12.5, 50 and 200 nM) of **7** (lanes 3-5) or same amount of DMSO as that in the ligand, added at the same time as the ligand (lane 2). A template (control) made of a scramble sequence of the same length in which five guanines have been mutated to thymines was used as internal control (lanes 6-10). Lane P: unreacted labelled primer. Vertical bars indicate G4-specific *Taq* polymerase stop sites: the corresponding sequence and G-tracts are shown aside. (B) Quantification of lanes 1-5 shown in panel A. Quantification of stop bands corresponding to G4 and of the full-length amplification product (FL) is shown. The gel was performed twice to confirm quantification results.

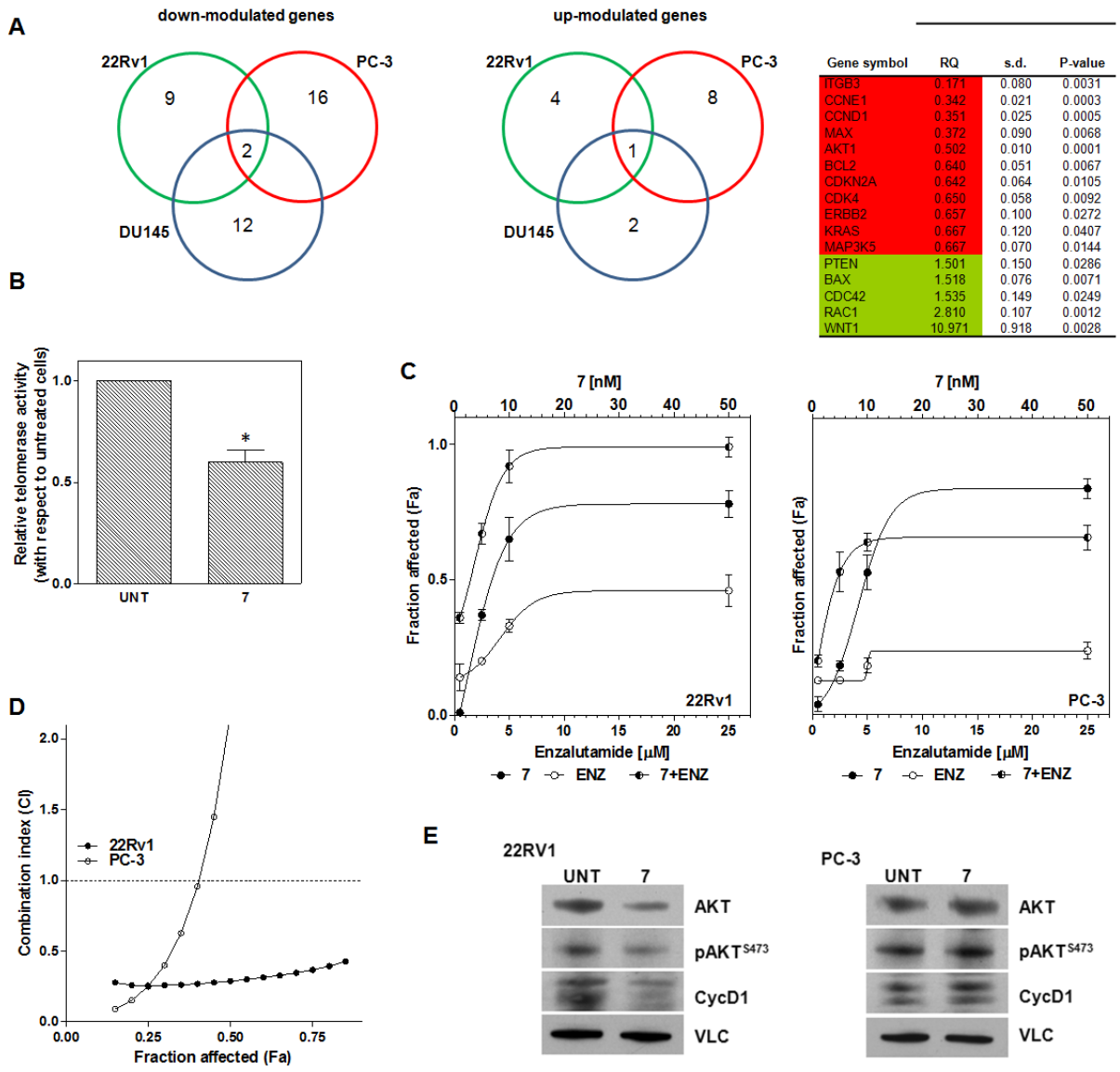

Figure 6. Effects of NDI **7** in AR-positive CRPC cells. (A) Graphic representation of the number of genes significantly ($P < 0.05$) down- and up-modulated (fold-change $\geq |1.5|$) in CRPC cells upon a 48-h exposure to NDI (IC_{50}). The graph on the right reports the list of differently expressed genes found in **7**-treated with respect to untreated (DMSO) 22Rv1 cells and showing a trend towards an opposite modulation in AR-negative cells. Expression data have been reported as RQ and represent mean values ± s.d. The complete list of tested genes is reported in Table S2. (B) Quantification of telomerase activity (see material and methods for details). Data have been reported as relative

telomerase activity in 22RV1 cells upon a 48-h exposure to **7** (IC_{50}) represents mean values ± s.d. *P < 0.05; **P < 0.02 (Student's t-test). UNT: Untreated (DMSO) cells. (C) Dose-response curves for 22Rv1 and PC-3 cells exposed to **7** (black circles), Enzalutamide (white circles) and **7**:Enzalutamide combination at the indicated concentrations. Data have been reported as the fraction affected (Fa) as a function of drug concentrations and represent mean values ± s.d. from at least three independent experiments. (D) Combination index (CI)-Fa plot showing the distribution of CI as a function of the fraction affected in 22RV1 (black circles) and PC-3 (white circles) cells exposed to the combination of **7**:Enzalutamide. CI < 1, = 1 (dashed line) and > 1 indicates synergism, additive effect and antagonisms, respectively (see materials and methods). (E) Representative western immunoblotting showing AKT1, phosphoAKT1(S473) and Cyclin D1 protein amounts in 22Rv1 and PC-3 cells exposed for 48 h to **7** (IC_{50}). Vinculin (VCL) was used as loading control. Cropped images of selected proteins are shown. UNT: untreated (DMSO) cells.

Scheme 1. Synthesis of intermediates and final water soluble NDI-dyads.

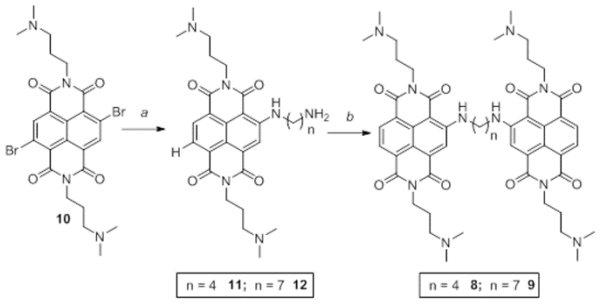

[a] 1,7-diaminoheptane or 1,4-diaminobutane 2.5 eq., CH_3CN, 75 °C, 4.5 h. NDI **11** (yield 80%).

[b] NDI **10** 1.1 eq., CH_3CN, 85 °C, 24 h. NDI dyads **8** (yield 51%) and **9** (yield 48%).

Table 1. Stabilization of AR1 and AR3 G4s (0.25 μM) by NDI derivatives (1 μM) measured by FRET assay at K^+ 100 mM.

	$\Delta T_{1/2}$ (°C) [a]		
Compound	**AR1 G4**	**AR3 G4**	**dsDNA**
1	11.0 ± 0.1	13.0 ± 0.8	5.1 ± 0.8
2	7.2 ± 1.5	10.0 ± 1.4	< 0.1
3	5.6 ± 0.3	9.0 ± 1.4	< 0.1
4	0.1 ± 0.1	0.4 ± 1.2	< 0.1
5	4.5 ± 0.7	9.3 ± 0.9	< 0.1
6	3.6 ± 0.3	6.0 ± 0.8	< 0.1
7	20.5 ± 0.7	31.0 ± 0.9	1.0 ± 0.2
8	11.3 ± 0.6	19.7 ± 0.5	1.9 ± 0.3
9	8.3 ± 1.0	17.0 ± 1.6	1.0 ± 0.2

[a] Variation in the oligonucleotide $T_{1/2}$ in the presence of the selected compounds. Data are reported as mean values ± s.d. from at least three independent experiments. In melting curves with a biphasic response, the $T_{1/2}$ of the second phase was used to calculate the $\Delta T_{1/2}$ value reported in the table.

Table 2. Steady state affinity of NDI derivatives towards AR1 measured by SPR analysis. Relative affinity was calculated as the ratio between K_D of compound **7** and K_D of the other compounds, and expressed as percentage.

Compound	**K_D (nM)** [a]	**Relative affinity**
1	41.2 ± 11.0	43%
2	34.2 ± 9.6	52%
3	21.4 ± 3.1	84%
4	ND	ND
5	43.9 ± 11.1	41%
6	38.3 ± 12.0	47 %
7	17.9 ± 2.0	100%
8	92.5 ± 24.1	19%
9	181.6 ± 34.2	10%

[a] Data are reported as mean values ± s.d. from two independent experiments

Table 3. IC_{50s} (μM) values obtained after a 48-h exposure of indicated cell lines to NDI derivatives[a]

Molecular characteristics[b]		PNT1A	DU145	PC-3	LNCaP	22Rv1
AR *(mRNA/Protein)*		–/–	–/–	–/–	+/+	+/+
PSA *(mRNA/Protein)*		–/–	–/–	–/–	+/+	+/–
Compound	**1**	0.59±0.05	3.88±1.53	6.32±0.34	3.40±0.10	2.43±0.29
	2	0.35±0.04	0.30±0.04	0.32±0.01	0.39±0.16	0.10±0.003
	3	0.13±0.01	0.55±0.09	0.34±0.01	0.59±0.04	0.97±0.02
	4	7.07±2.38	>>10	>10	>>10	7.67±1.15
	5	1.44±0.25	>10	>>10	3.04±0.08	3.69±0.41
	6	1.37±0.25	>>10	>>10	10.33±1.36	>>10
	7	0.28±0.03	0.08±0.01	0.18±0.01	0.14±0.05	0.010±0.001
	8	2.48±0.82	3.39±0.48	10.11±3.09	1.93±0.07	>>10
	9	1.89±0.57	2.19±0.14	>>10	6.56±0.17	3.45±0.16

[a]Data have been obtained from dose-response curves and reported as mean values ± s.d. from at least three independent experiments;

[b]LNCaP cells bear the AR full length with the point mutation T877A; 22Rv1 cells bear the AR full length with the point mutation H875Y and express constitutively active AR variants; they do not express PSA protein (see refs. 1 and 51-54).

Table of Contents Graphic